Ozone_cci+

Algorithm Theoretical Basis Document (ATBD)

Date: 17/03/2025

Version: 3.2

WP Manager: R. Siddans

WP Manager Organization: STFC Rutherford Appleton Laboratory

Other partners: DLR-IMF, KNMI, RAL, ULB, UBR, FMI

DOCUMENT PROPERTIES

Title	Algorithm Theoretical Basis Document (ATBD)
Reference	Ozone_cci+_D1.2_ATBD_v3.2
Issue	3
Revision	2
Status	Final
Date of issue	17 March 2025
Document type	D2.1

	FUNCTION	NAME	DATE	SIGNATURE
LEAD AUTHOR	Project partner	Richard Siddans	04/11/2024	
CONTRIBUTING AUTHORS	Project partner	M. Coldewey-Egbers, V. Sofieva, R. van der A, C. Wespes, C. Arioso K. Heue	04/11/2024	
REVIEWED BY	Science leader	Daan Hubert	23/12/2024	
APPROVED BY	ESA	Michael Eisinger	05/03/2025	
ISSUED BY	Project partner	Richard Siddans	17/03/2025	

DOCUMENT CHANGE RECORD

Issue	Revision	Date	Modified items	Observations
0	0	14/2/2020	Initial template	Creation of document
1	0	7/5/2020	First issued version	
1	1	8/3/2021	Modifications in response to ESA comments on version 1.0: Fig 3 (now 2.3) update (and now shows to TROPOMI - GOME2C, consistent with fig 2.2) p23: Reference to the chorine activation term added. Ch 3.2.7: Averaging kernel quality check clarified. p32: Clarified text reference to x vs r. p33: Clarification has been added regarding use of x and x-hat. Ch 4.2.3 New section added. Editorial: Table of contents alignment fixed MLS acronym added Some minor typos fixed Rationalised numbering of equations figures and tables throughout.	
2	0	5/11/2021	Updates to Sects. 2.1, 3.2, 4.2, 4.4.	
2	1	24/1/2023	Inclusion of GOP-ECV algorithm (Sect. 3.1)	
3	0	30/1/2023	First version produced in CCI+ phase 2. Only contains sections relevant to algorithms developed in this phase. Sections related to GOP-ECV, IASI FORLI, Limb profile ECV merging are updated. Section on tropospheric ozone is added.	

Issue	Revision	Date	Modified items	Observations
3	1	23/12/2024	S3.1 Updates (mainly the figures) related to GOP-ECV; S3.3 Updates to IASI algorithm description S4.1 Updates to OMPS-LP S5.1 CCD scheme: More detailed description of the harmonisation scheme	
3	2	17/03/2025	Document header	Approved by ESA

Executive Summary

The Algorithm Theoretical Basis Document (ATBD, deliverable D2.1 in Ozone_cci+) describes the algorithms developed in CCI+ phase 2 (Jul 2022 – Jan 2025) for total ozone columns, nadir-based ozone profiles, limb-based ozone profiles and tropospheric ozone columns.

A series of new algorithms will be developed with a focus on both level-2 and level-3 data products, as follows.

- Total Ozone ECV Retrieval Algorithms
    - Multi-Sensor-Reanalysis scheme (KNMI)
- Nadir Profile ECV Retrieval Algorithms
    - GOME-type Ozone Profile ECV merging algorithm (GOP-ECV) (DLR)
    - RAL nadir profile ECV retrieval algorithms (RAL)
    - IASI FORLI Ozone profile retrieval algorithm (ULB)
    - IASI merging algorithm (ULB)
    - Combined uv/vis/thermal-ir retrieval algorithm (RAL)
- Limb profile ECV Retrieval / Merging Algorithm
    - OMPS-LP retrieval algorithm (IUP)
    - High-resolution gap-free dataset of ozone profiles (FMI)
- Tropospheric Ozone
    - Merging of tropical GOME-type CCD data (GTTO-ECV scheme) (DLR)
    - Global tropospheric ozone from nadir and multiple limb sensors (FMI)

Table of Contents

1 Purpose and scope

1.1 Purpose

This document describes the algorithms used in the Ozone_cci+ Phase 2, addressing total ozone columns, nadir-based ozone profiles, limb-based ozone profiles and tropospheric ozone columns.

1.2 Scope

The scope of the ATBD is to document algorithms used in phase 2 of the CCI+ project (Jul 2022-Jan 2025), with particular emphasis on algorithm features which are new in this phase. Where algorithms are already described by existing ATBDs or similar documents, references are made to these documents and only a brief overview of the algorithmic basis is given.

1.3 Applicable documents

[AD-1] Data Standards Requirements for CCI Data Producers. Latest version at time of writing is v1.2: ref. CCI-PRGM-EOPS-TN-13-0009, 9 March 2015, available online at: http://cci.esa.int/sites/default/files/CCI_Data_Requirements_Iss1.2_Mar2015.pdf

[AD-2] CCI Data Policy v1.1. Available online at: https://earth.esa.int/documents/10174/1754357/RD-7_CCI_Data_Policy_v1.1.pdf

1.4 References documents

[RD-1] GCOS Climate Monitoring Principles, November 1999, reproduced in [RD-5], p48.

[RD-2] Guideline for the Generation of Satellite-based Datasets and Products meeting GCOS Requirements, GCOS Secretariat, GCOS-128, March 2009 (WMO/TD No. 1488). Available online at: http://library.wmo.int

[RD-3] Quality assurance framework for earth observation (QA4EO): http://qa4eo.org

[RD-4] EU Research Programmes on Space and Climate: Horizon 2020 (H2020), (http://ec.europa.eu/programmes/horizon2020/en/h2020-section/space, https://ec.europa.eu/programmes/horizon2020/en/h2020-section/climate-action-environment-resource-efficiency-and-raw-materials) and Copernicus (http://www.copernicus.eu/).

[RD-5] The Global Observing System for Climate: Implementation Needs, GCOS-200, October 2016. Available online at: http://library.wmo.int

[RD-6] Status of the Global Observing System for Climate, GCOS-195, October 2015. Available online at: http://library.wmo.int

[RD-7] Joint Committee for Guides in Metrology, 2008, Evaluation of measurement data — Guide to the expression of uncertainty in measurement (GUM), JGCM 100: 2008. Available online at http://www.bipm.org/en/publications/guides/gum.html.

[RD-8] Copernicus Space Component: http://www.esa.int/Our_Activities/Observing_the_Earth/Copernicus/Space_Component

[RD-9] User requirements for monitoring the evolution of stratospheric ozone at high vertical resolution (Operoz), 2015, ESA Expro contract 4000112948/14/NL/JK. Available online at: http://projects.knmi.nl/capacity/Operoz/Operoz_final_report_with_exec_summary_1mar2015.pdf

[RD-10] K. Bogumil, J. Orphal, T. Homann, S. Voigt, P. Spietz, O.C. Fleischmann, A. Vogel, M. Hartmann, H., Bovensmann, J. Frerick, and J.P. Burrows, "Measurements of molecular absorption spectra with the SCIAMACHY pre-flight model: Instrument characterization and reference data for atmospheric remote sensing in the 230-2380 nm region", J. Photochem. Photobiol. A: Chem. 157, 167-184 (2003); DOI: 10.1016/S1010-6030(03)00062-5

[RD-11] Boynard, A., et al.: Validation of the IASI FORLI/EUMETSAT O3 products using satellite (GOME-2), ground-based (Brewer-Dobson, SAOZ, FTIR) and ozonesonde measurements, Atmos. Meas. Tech.,https://doi.org/10.5194/amt-11-5125-2018 , 2018.

[RD-12] Cariolle, D. and Teyssèdre, H.: A revised linear ozone photochemistry parametrization for use in transport and general circulation models: Multi-annual simulations, Atmos. Chem. Phys. Discuss., 7, 1655–1697, 2007.

[RD-13] Chance, K., Burrows, J et al., Satellite measurements of atmospheric ozone profiles, including tropospheric ozone, from ultraviolet/visible measurements in the nadir geometry: a potential method to retrieve tropospheric ozone, J. Quant. Spectrosc. Radiat. Transfer Vol. 51. No. 4, pp. 461476, 1997

[RD-14] Chen, Z., DeLand, M., and Bhartia, P. K.: A new algorithm for detecting cloud height using OMPS/LP measurements, Atmos. Meas. Tech., 9, 1239–1246, https://doi.org/10.5194/amt-9-1239-2016, 2016.

[RD-15] Chinaud, J., et al.: IASI-C L1 Cal/Val System performance synthesis. EUMETSAT Technical Note IA-NT-0000-4477-CNES, https://www.EUMETSAT.int/website/home/News/DAT_4439637.html, 2019.

[RD-16] Coldewey-Egbers, M., Loyola, D. G., Koukouli, M., Balis, D., Lambert, J.-C., Verhoelst, T., Granville, J., van Roozendael, M., Lerot, C., Spurr, R., Frith, S. M., and Zehner, C.: The GOME-type Total Ozone Essential Climate Variable (GTO-ECV) data record from the ESA Climate Change Initiative, Atmos. Meas. Tech., 8, 3923–3940, https://doi.org/10.5194/amt-8-3923-2015, 2015.

[RD-17] Coldewey-Egbers, M., Loyola, D., Labow, G., and Frith, S.: Comparison of GTO-ECV and Adjusted-MERRA total ozone columns from the last two decades and assessment of interannual variability, Atmos. Meas. Tech. Discuss., https://doi.org/10.5194/amt-2019-297, in review, 2019.

[RD-18] Eskes, H. J., van Velthoven, P. F. J., Valks, P. J. M. and Kelder, H. M.: Assimilation of GOME total ozone satellite observations in a three-dimensional tracer transport model, Q. J. R. Meteorol. Soc., 129, 1663-1681, 2003.

[RD-19] Garane, K., Lerot, C., Coldewey-Egbers, M., Verhoelst, T., Koukouli, M.E., Zyrichidou, I., Balis, D.S., Danckaert, T., Goutail, F., Granville, J., Hubert, D., Keppens, A., Lambert, J.-C., Loyola, D., Pommereau, J.-P., Van Roozendael, M., and Zehner, C.: Quality assessment of the Ozone_cci Climate Research Data Package (release 2017) – Part 1: Ground-based validation of total ozone column data products, Atmos. Meas. Tech., 11, 1385-1402, doi:10.5194/amt-11-1385-2018, 2018.

[RD-20] Garane, K., Koukouli, M.-E., Verhoelst, T., Lerot, C., Heue, K.-P., Fioletov, V., Balis, D., Bais, A., Bazureau, A., Dehn, A., Goutail, F., Granville, J., Griffin, D., Hubert, D., Keppens, A., Lambert, J.-C., Loyola, D., McLinden, C., Pazmino, A., Pommereau, J.-P., Redondas, A., Romahn, F., Valks, P., Van Roozendael, M., Xu, J., Zehner, C., Zerefos, C., and Zimmer, W.: TROPOMI/S5P total ozone column data: global ground-based validation and consistency with other satellite missions, Atmos. Meas. Tech., 12, 5263–5287, https://doi.org/10.5194/amt-12-5263-2019, 2019.

[RD-21] Hermans, C.: O4 absorption cross-sections at 296K (335.59–666.63 nm), online available from: http://spectrolab.aeronomie.be/index.htm (last accessed 15 January 2011), 2011.

[RD-22] Hollmann, R., et al., The ESA climate change initiative: Satellite data records for essential climate variables. American Meteorological Society. Bulletin, Vol. 94, No. 10, 2013, p. 1541-1552.

[RD-23] Hurtmans, D,. et al.: FORLI radiative transfer and retrieval code for IASI, Journal of Quantitative Spectroscopy and Radiative Transfer, https://doi.org/10.1016/j.jqsrt.2012.02.03, 2012.

[RD-24] Keppens, A., J.-C. Lambert, J. Granville, D. Hubert, T. Verhoelst, S. Compernolle, B. Latter, B. Kerridge, R. Siddans, A. Boynard, J. Hadji-Lazaro, C. Clerbaux, C. Wespes, D. R. Hurtmans, P. F. Coheur, J. van Peet, R. van der A, K. Garane, M. E. Koukouli, D. S. Balis, A. Delcloo, R. Kivi, R. Stübi, S. Godin-Beekmann, M. Van Roozendael, C. Zehner: Quality assessment of the Ozone_cci Climate Research Data Package (release 2017): 2. Ground-based validation of nadir ozone profile data products, Atmos. Meas. Tech., 11, 3769–3800,https://doi.org/10.5194/amt-11-3769-2018, 2018.

[RD-25] Kerr, J. B.: New methodology for deriving total ozone and other atmospheric variables from Brewer spectrophotometer direct sun spectra, J. Geophys. Res., 107(D23), 4731, doi:10.1029/2001JD001227, 2002.

[RD-26] Koukouli, M. E., Lerot, C., Granville, J., Goutail, F., Lambert, J.-C., Pommereau, J.-P., Balis, D., Zyrichidou, I., Van Roozendael, M., Coldewey-Egbers, M., Loyola, D., Labow, G., Frith, S., Spurr, R. and Zehner, C.: Evaluating a new homogeneous total ozone climate data record from OME/ERS-2, SCIAMACHY/Envisat, and GOME-2/Metop-A, J. Geophys. Res. Atmos., 120(23), 12,296-2,312, doi:10.1002/2015JD023699, 2015.

[RD-27] Kramarova, N. A., Bhartia, P. K., Jaross, G., Moy, L., Xu, P., Chen, Z., DeLand, M., Froidevaux, L., Livesey, N., Degenstein, D., Bourassa, A., Walker, K. A., and Sheese,

P.: Validation of ozone profile retrievals derived from the OMPS LP version 2.5 algorithm against correlative satellite measurements, Atmos. Meas. Tech., 11, 2837–2861, https://doi.org/10.5194/amt-11-2837-2018, 2018.

[RD-28] Krol, M., S. Houweling, B. Bregman, M. van den Broek, A. Segers, P. van Velthoven, W. Peters, F. Dentener and P. Bergamaschi: The two-way nested global chemistry-transport zoom model TM5: algorithm and applications, Atmos. Chem. Phys., 5, 417-432, 2005.

[RD-29] Lerot, C., et al. "Homogenized total ozone data records from the European sensors GOME/ERS-2, SCIAMACHY/Envisat and GOME-2/Metop-A." J. Geophys. Res., 119, 3, 1639-1662, doi:10.1002/2013JD020831, 2014.

[RD-30] Loughman, R., Bhartia, P. K., Chen, Z., Xu, P., Nyaku, E., and Taha, G.: The Ozone Mapping and Profiler Suite (OMPS) Limb Profiler (LP) Version 1 aerosol extinction retrieval algorithm: theoretical basis, Atmos. Meas. Tech., 11, 2633–2651, https://doi.org/10.5194/amt-11-2633-2018, 2018.

[RD-31] Merchant, C., et al., 2017, Uncertainty information in climate data records from Earth observation, Earth Syst. Sci. Data Discuss., vol. 9, p511-527.

[RD-32] Miles, G.M., R. Siddans, B. J. Kerridge, B. G. Latter, and N. A. D. Richards, Tropospheric ozone and ozone profiles retrieved from GOME-2 and their validation, AMT, doi:10.5194/amt-8-385-2015

[RD-33] Munro, R., R. Siddans, W.J. Reburn, and B.J. Kerridge. "Direct measurement of tropospheric ozone distributions from space." Nature 392 (1998): 168-171.

[RD-34] Newman, P. A., Daniel, J. S., Waugh, D. W., and Nash, E. R.: A new formulation of equivalent effective stratospheric chlorine (EESC), Atmos. Chem. Phys., 7, 4537–4552, https://doi.org/10.5194/acp-7-4537-2007, 2007.

[RD-35] Ohring, G., 2007: Achieving Satellite Instrument Calibration for Climate Change. Eos, Transactions, American Geophysical Union, Vol. 88, Issue 11.

[RD-36] Pedergnana, M., D. Loyola, A. Apituley, M. Sneep, P. Veefkind, Sentinel-5 precursor/TROPOMI L2 Product User Manual O3 Total Column, S5P-L2-DLR-PUM-400A, Issue 01-01-01, 16-07-2018

[RD-37] Petropavlovskikh, I., Godin-Beekmann, S., Hubert, D., Damadeo, R., Hassler, B., and Sofieva, V.: SPARC/IO3C/GAW report on Long-term Ozone Trends and Uncertainties in the Stratosphere, SPARC/IO3C/GAW, SPARC Report No. 9, WCRP-17/2018, GAW Report No. 241, https://doi.org/10.17874/f899e57a20b, 2019. a, b, c, d, e, f, g, h

[RD-38] Prather, M. J.: Numerical advection by conservation of ozone data in weather-prediction models, Q.J.R.Meteorol. Soc., 122, 1545-1571, 1986.

[RD-39] Rahpoe, N., A. Laeng, G. Stiller, M. Weber *(eds)* and R. van der A, C. Adams, P. Bernath, T. von Clarmann, M. Coldewey-Egbers, D. Degenstein, A. Dudhia, R. Hargreaves, C. Lerot, D. Loyola, J. van Peet, V. Sofieva, J. Tamminen, J. Urban, M. Van Roozendael, T. Danckaert, R. Astoreca, K.-P. Heue, P. Sheese, K. Walker and S.

Tukiainen, Ozone_cci Phase-II Algorithm Theoretical Basis Document (ATBD), Version 2, Issue 0, Revision 0, Ozone_cci_ATBD_Phase2_V2, December 2017.

[RD-40] Redondas, A. and Cede, A.: Brewer algorithm sensitivity analysis, SAUNA workshop, Puerto de la Cruz, Tenerife, November, 2006.

[RD-41] Serdyuchenko, A., Gorshelev, V., Weber, M., Chehade, W., and Burrows, J. P.: High spectral resolution ozone absorption cross-sections – Part 2: Temperature dependence, Atmos. Meas. Tech., 7, 625–636, https://doi.org/10.5194/amt-7-625-2014, 2014

[RD-42] Siddans, R. Height Resolved Ozone Retrievals from Global Ozone Monitoring Experiment. PhD Thesis, University of Reading, 2003

[RD-43] Siddans, R. et al, Sentinel 5 L2 Prototype Processors, Algorithm Theoretical Basis Document: Ozone Profile. RAL-ESA-S5L2PP-ATBD-001, Version 3.1, 17 May 2019

[RD-44] Siddans, R., CCI+ Water Vapour: ATBD Part 2 - IMS L2 Product, Ref: CCIWV.REP.005, Issue 1, 2019

[RD-45] Siddans, R. et al, Sentinel 4 Level 2 ATBD: Tropospheric Ozone, Document ID S4-L2-RAL-ATBD-2003, Issue 2.2 , Date: 2020-04-21

[RD-46] Sofieva, V. F., Kyrölä, E., Laine, M., Tamminen, J., Degenstein, D., Bourassa, A., Roth, C., Zawada, D., Weber, M., Rozanov, A., Rahpoe, N., Stiller, G., Laeng, A., von Clarmann, T., Walker, K. A., Sheese, P., Hubert, D., van Roozendael, M., Zehner, C., Damadeo, R., Zawodny, J., Kramarova, N., and Bhartia, P. K.: Merged SAGE II, Ozone_cci and OMPS ozone profile dataset and evaluation of ozone trends in the stratosphere, Atmos. Chem. Phys., 17, 12533–12552, https://doi.org/10.5194/acp-17-12533-2017, 2017.

[RD-47] Spurr, R. "LIDORT and VLIDORT: Linearized pseudo-spherical scalar and vector discrete ordinate radiative transfer models for use in remote sensing retrieval problems." In Light Scattering Reviews, Volume 3, by A. A. Kokhanovsky (ed.). Springer, 2008.

[RD-48] Spurr, R., V. Natraj, C. Lerot, M. Van Roozendael, and D. Loyola. "Linearization of the Principal Component Analysis method for radiative transfer acceleration: Application to retrieval algorithms and sensitivity studies." J. Quant. Spectrosc. Radiat. Transfer 125 (2013): 1-17.

[RD-49] Spurr, R., D. Loyola, M. Van Roozendael, C. Lerot, K.-P. Heue, J. Xiu, S5P/TROPOMI Total Ozone ATBD, S5P-L2-DLR-ATBD-400A, Issue 2.0, 23/08/2019.

[RD-50] van der A, R.J., M.A.F. Allaart and H.J. Eskes, Multi sensor reanalysis of total ozone Atm. Chem. Phys., 2010, 10, 11277-11294, doi:10.5194/acp-10-11277-2010.

[RD-51] van der A, R. J., Allaart, M. A. F., and Eskes, H. J.: Extended and refined multi sensor reanalysis of total ozone for the period 1970-2012, Atmos. Meas. Tech., 8, 3021-3035, doi:10.5194/amt-8-3021-2015, 2015.

[RD-52] Van Roozendael, M., et al. "Fifteen years of GOME/ERS2 total ozone data: the new direct-fitting GOME Data Processor (GDP) Version 5: I. Algorithm Description." J. Geophys. Res. 117 (2012): D03305

[RD-53] Van Rozendael, M., et al., C3S Ozone Algorithm Theoretical Basis Document (ATBD), Version 1.1a, 3S_312b_Lot2.1.1.2_201902_ATBD_v1.1a, 8/4/2019.

[RD-54] Weber, M et al, Ozone CCI ATBD, Issue 0 - Revision 00 - Status: Final, Date of issue: Dec 7, 2017

[RD-55] Weber, M., Coldewey-Egbers, M., Fioletov, V. E., Frith, S. M., Wild, J. D., Burrows, J. P., Long, C. S., and Loyola, D.: Total ozone trends from 1979 to 2016 derived from five merged observational datasets – the emergence into ozone recovery, Atmos. Chem. Phys., 18, 2097–2117, https://doi.org/10.5194/acp-18-2097-2018, 2018.

[RD-56] WMO (World Meteorological Organization), Scientific Assessment of Ozone Depletion: 2014, World Meteorological Organization, Global Ozone Research and Monitoring Project-Report No. 55, 416 pp., Geneva, Switzerland, 2014.

[RD-57] WMO (World Meteorological Organization), Scientific Assessment of Ozone Depletion: 2018, Global Ozone Research and Monitoring Project – Report No. 58, 588 pp., Geneva, Switzerland, 2018.

[RD-58] Zawada, D. J., Rieger, L. A., Bourassa, A. E., and Degenstein, D. A.: Tomographic retrievals of ozone with the OMPS Limb Profiler: algorithm description and preliminary results, Atmos. Meas. Tech., 11, 2375–2393, https://doi.org/10.5194/amt-11-2375-2018, 2018.

[RD-59] Arosio, C., Rozanov, A., Malinina, E., Eichmann, K.-U., von Clarmann, T., and Burrows, J. P.: Retrieval of ozone profiles from OMPS limb scattering observations, Atmos. Meas. Tech., 11, 2135–2149, https://doi.org/10.5194/amt-11-2135-2018, 2018.

[RD-60] D. Hurtmans, P.-F. Coheur, C. Wespes, L. Clarisse, O. Scharf, C. Clerbaux, J. Hadji-Lazaro, M. George, S. Turquety, FORLI radiative transfer and retrieval code for IASI , March 2012. https://doi.org/10.1016/j.jqsrt.2012.02.036

[RD-61] Thomas August, Dieter Klaes, PeterSchlüssel, TimHultberg, MarcCrapeau, ArlindoArriaga, AnneO'Carroll, Dorothée Coppens. RoseMunro, XavierCalbet, IASI on Metop-A: Operational Level 2 retrievals after five years in orbit, https://doi.org/10.1016/j.jqsrt.2012.02.028

[RD-62] Sofieva, V. F., Szeląg, M., Tamminen, J., Kyrölä, E., Degenstein, D., Roth, C., Zawada, D., Rozanov, A., Arosio, C., Burrows, J. P., Weber, M., Laeng, A., Stiller, G. P., von Clarmann, T., Froidevaux, L., Livesey, N., van Roozendael, M., and Retscher, C.: Measurement report: regional trends of stratospheric ozone evaluated using the MErged GRIdded Dataset of Ozone Profiles (MEGRIDOP), Atmos. Chem. Phys., 21, 6707–6720, https://doi.org/10.5194/acp-21-6707-2021, 2021

[RD-63] Heue, K.-P., et al.: Trends of tropical tropospheric ozone from 20 years of European satellite measurements and perspectives for the Sentinel-5 Precursor, Atmos. Meas. Tech., 9, 5037–5051, https://doi.org/10.5194/amt-9-5037-2016, 2016.

[RD-64] Valks, P., et al. "Tropical tropospheric ozone column retrieval for GOME-2", Atmos. Meas. Tech., 7, 2513-2530, doi:10.5194/amt-7-2513-2014, 2014.

[RD-65] Sofieva, V. F., Hänninen, R., Sofiev, M., Szeląg, M., Lee, H. S., Tamminen, J., and Retscher, C.: Synergy of Using Nadir and Limb Instruments for Tropospheric Ozone Monitoring (SUNLIT), Atmos. Meas. Tech., 15, 3193–3212, https://doi.org/10.5194/amt-15-3193-2022, 2022.

1.5 Acronyms

ACE-FTS	Atmospheric Chemistry Experiment – Fourier Transform Spectrometer
ATBD	Algorithm Theoretical Basis Document
BIRA-IASB	Belgian Institute for Space Aeronomy
CCI	Climate Change Initiative
CDR	Climate Data Record
C3S	Copernicus Climate Change Service
DLR	German Aerospace Centre
ECMWF	European Centre for Medium-range Weather Forecast
ECV	Essential Climate Variable
EVISAT	Environmental Satellite (ESA)
EO	Earth Observation
ESA	European Space Agency
EU	European Union
EUMETSAT	European Organisation for the Exploitation of Meteorological Satellites
FMI	Finnish Meteorological Institute
GAW	Global Atmosphere Watch
GCOS	Global Climate Observation System
GOME	Global Ozone Monitoring Experiment (aboard ERS-2)
GOME-2	Global Ozone Monitoring Experiment – 2 (aboard MetOp-A)
GOMOS	Global Ozone Monitoring by Occultation of Stars
GOP	GOME-type Ozone Profile
GTO	GOME-type Total Ozone
IASI	Infrared Atmospheric Sounding Interferometer
KNMI	Royal Netherlands Meteorological Institute
MetOp	Meteorological Operational Platform (EUMETSAT)
MIPAS	Michelson Interferometer for Passive Atmospheric Sounding
MLS	Microwave Limb Sounder
NASA	National Aeronautics and Space Administration
NDACC	Network for the Detection of Atmospheric Composition Change
OMI	Ozone Monitoring Instrument (aboard EOS-Aura)
OSIRIS	Optical and Spectroscopic Remote Imaging System (aboard Odin)

RAL	Rutherford Appleton Laboratory
SCIAMACHY	Scanning Imaging Absorption Spectrometer for Atmospheric CHartographY
TOMS	Total Ozone Mapping Spectrometer
UV	Ultraviolet

2 Total Ozone ECV Retrieval Algorithms

2.1 Multi-Sensor-Reanalysis scheme (KNMI)

This section is not updated since ATBD V2.1 from CCI+ phase 1.

2.1.1 Introduction MSR algorithm

A single coherent total ozone dataset, called the Multi Sensor Reanalysis (MSR), has been created from all available ozone column data measured by polar orbiting satellites in the near-ultraviolet Huggins band in the last thirty years. All available total ozone satellite retrieval datasets have been used in the MSR. As first step a bias correction scheme is applied to all satellite observations, based on independent ground-based total ozone data from the World Ozone and Ultraviolet Data Center. The correction is a function of solar zenith angle, viewing angle, time (trend), and effective ozone temperature. As second step data assimilation was applied to create a global dataset of total ozone analyses. The data assimilation method is a sub-optimal implementation of the Kalman filter technique, and is based on a chemical transport model driven by ECMWF meteorological fields. The chemical transport model provides a detailed description of (stratospheric) transport and uses parameterisations for gas-phase and ozone hole chemistry. The MSR dataset is available on a grid of a 0.5x0.5 degrees with a sample frequency of 6 hours for the complete time period.

Constructing the MSR level 2 data set

Creating a consistent and coherent assimilated dataset of use for trend studies requires that systematic offsets of each one of the satellite retrieval products is small. A practical way to accomplish this is to choose a reference dataset which is available for the full reanalysis period, and subsequently correct the systematic effects in the satellite datasets to bring them in line with this reference. As reference we use the ground measurements from Brewer and Dobson monitoring stations, which are present for the full 30-year period.

First of all, these ground measurements will also show biases, depending on geometry, meteorological variability and ozone profile. The direct Sun measurement method used by the Brewer instruments is very sensitive to small details in the ozone absorption cross section, and the various available laboratory measurements of the ozone absorption coefficients give totally different dependencies of the retrieved total ozone values as function of the effective ozone temperature [RD-40]. Kerr (2002) [RD-25] has developed a new methodology for deriving total ozone and effective ozone temperature values from the observations made with a Brewer instrument. He concludes that the effective ozone temperature has little effect on the amount of ozone derived with the standard algorithm. So in this study the data from the Brewer network has been adopted as a primary reference. The Dobson data compared to Brewer data show a temperature dependence. Therefore, the Dobson data has been corrected for effective ozone temperature and added to this reference data set.

For each satellite product an “overpass” dataset has been created for each ground instrument in our list. The overpass value for an orbit is the satellite observation that has the centre of its footprint closest to the ground station. For each satellite product a maximum allowed distance between the

centre of the ground pixel and the ground station was defined. This number is typically 50-200 km depending on the ground pixel size. Apart from the local date/time and the total ozone value, auxiliary data is also recorded, like the measurement error, the Solar Zenith Angle (SZA), the Viewing Zenith Angle (VZA), cloud properties and the distance from the centre of the footprint to the ground station. From all the overpasses each day only one is selected and used. This is the one with the smallest reported observation error or the one closest to the ground station if the observation error is not available.

For the purpose of data assimilation it is relevant to reduce offsets, trends and long-term variations in the satellite data, so that the data can be used as input to the assimilation scheme without biases and with known standard deviations. The satellite data set corrections are based on a few relevant regression coefficients fitted for the overpass time series of all stations together. By fitting all data together regional biases that may be caused by offsets of individual ground instruments are avoided.

The ozone differences (satellite minus ground observation) show a clear seasonal cycle. This led to the choice of SZA and effective ozone temperature as fit parameter, as these imply a clear seasonal component. Some of the satellite products show a clear trend in time, so date/time is another obvious choice. The Viewing Zenith Angle (VZA) is also used as fit parameter. These are all critical parameters in the retrieval schemes and therefore constitute a satisfying choice to estimate systematic biases. A ground-station dependent offset was allowed when the regression coefficients were computed. This has been done to reduce the effect (e.g. spurious trends) of “appearing” and “disappearing” ground stations during the lifetime of the satellite instrument from the results. Thus, the total number of fit parameters is in the order of 150 per satellite dataset. A basic assumption is that all the corrections are additive to the total ozone amount.

Based on the calculated corrections the merged MSR level 2 dataset has been created. The original satellite datasets were read, filtered for bad data and corrected, and finally merged into a single time ordered dataset. Essential information in the MSR level 2 dataset is time, location, satellite product index and ozone.

Data assimilation

The satellite instrument observations are combined with meteorological, chemical and dynamical knowledge of the atmosphere by using data assimilation. The data assimilation scheme used here is called TM3DAM and is described in [RD-18]. The chemistry-transport model used in this data assimilation is a simplified version of TM5 [RD-28], which is driven by ECMWF analyses of wind, pressure and temperature fields. As input the MSR ozone values and the estimates of the measurement uncertainty are used.

The three-dimensional advection of ozone is described by the flux-based second order moments scheme of Prather et al. (1986) [RD-38]. The model is driven by 6-hourly meteorological fields (wind, surface pressure, and temperature) of the medium-range meteorological analyses of the ECMWF. The assimilation is using the ERA interim or ERA5 reanalysis whenever available. The ECMWF hybrid layers between 0.01 hPa and the surface have been converted into the 44 layers used in TM3DAM. The horizontal resolution of the model version used in this study is 1 x 1 degrees. This resolution is compensated by the practically non-diffusive Prather scheme (with 10

explicit ozone tracers for each grid cell), which allows the model to produce ozone features with a fair amount of detail.

Ozone chemistry in the stratosphere is described by the Cariolle version 2.9 parameterisation [RD-12]. This consists of a linearization of the gas-phase chemistry with respect to production and loss, the ozone amount, temperature and UV radiation. In addition, a second parameterization scheme accounts for heterogeneous ozone loss. This scheme introduces a three-dimensional chlorine activation tracer, which is formed when the temperature drops below the critical temperature of polar stratospheric cloud formation. Ozone breakdown occurs in the presence of the chlorine activation tracer, depending on the presence of sunlight. The rate of ozone decrease is described by an exponential decay, with a rate proportional to the amount of activation tracer below the critical temperature and with a minimal decay time of 12 days. The cold tracer is deactivated when light is present with a time scale of respectively 5 and 10 days on the Northern and Southern hemisphere.

The total ozone data are assimilated in TM3DAM by applying a parameterized Kalman filter technique. In this approach the forecast error covariance matrix is written as a product of a time independent correlation matrix and a time-dependent diagonal variance. The various parameters in the approach are fixed and are based on the forecast minus observation statistics accumulated over the period of one year (2000) using GOME observations. This approach produces detailed and realistic time- and space-dependent forecast error estimates, which is included in the MSR level 4 product.

More details of the MSR algorithm can be found in [RD-51] and [RD-50].

2.1.2 Algorithm update to extend the MSR data set into the past

Heterogeneous chemistry

An EESC dependent heterogeneous chemical destruction of stratospheric ozone factor has been be incorporated within the exponent of the ozone depletion term within the Braesicke scheme.

The EESC correction factor fCFC is calculated according

$$F_{CFC} = (EESC/EESC_{max})^2 \text{ where } EESC_{max} = 4092.8508$$

Equation 2-1

The EESC values are derived in [RD-34] and are calculated for the period 1957-2020.

Solar Zenith Angle dependence of photolysis factor

A linear correction factor fSZA for photolysis during twilight has been derived. The twilight is the zone with a Solar Zenith Angle (SZA) between 85 and 94 degree.

$$f_{SA} = (94.0 - SZA)/(94.0 - 85.0) \text{ for SZA between 84.0-95.0 degree}$$

Equation 2-2

This factor has been multiplied with the chlorine activation term [RD-18].

Error correlation length

For sparse observations it is likely that the error correlation length in the spatial distribution of assimilated ozone is different. Therefore the correlation length is determined by assimilating ozone using only sparse Dobson observations in 2017. The resulting ozone has been compared with the MSR2 ozone distribution that represent the “true” ozone distribution. From analysing these datasets we conclude that the correlation length is about 800 km.

3 Nadir Profile ECV Retrieval Algorithms

3.1 GOME-type Ozone Profile - Essential Climate Variable (GOP-ECV) (DLR)

Work within CCI+ Phase-I focused on the development of a merged ozone profile climate data record based on the same satellite sensors as the well-established total column product GTO-ECV (see Phase I ATBD). The approach, that is applied to the ozone profiles, consists of two main steps: (1) merging the time series of the individual sensors into a combined product and (2) harmonization of the combined record with respect to the GTO-ECV total columns in order to achieve broad consistency between both data sets.

3.1.1 Ozone profile merging algorithm

At first, the individual gridded monthly level-3 ozone profile data are merged into a combined record. The level-3 partial column data are based on the level-2 data retrieved with the RAL nadir profile retrieval scheme as described in the next section (Sect. 3.2). Data from five sensors are included: GOME (1995-2011), SCIAMACHY (2002-2012), OMI (2004-present), GOME-2A (2007-2021), and GOME-2B (2013-present). The values given in parenthesis denote the time periods which are covered by the sensors. These sensors are also used to create the GTO-ECV record. Note that data from TROPOMI and GOME-2C are not yet included in this first version of GOP-ECV. The merging is based on deseasonalized anomalies and similar to the method proposed by Sofieva et al. (2021) [RD-62]. Deseasonalized anomalies $\Delta O_{3,i}(\varphi,\lambda,z,t)$ at latitude φ, longitude λ, altitude z, and month t are computed for the time series of all individual instruments *i* following:

$$\Delta O_{3,i}(\varphi,\lambda,z,t) = O_{3,i}(\varphi,\lambda,z,t) - O_{3,i,c}(\varphi,\lambda,z,m),$$

Equation 3-3

where $O_{3,i}(\varphi,\lambda,z,t)$ is the monthly mean ozone profile. $O_{3,i,c}(\varphi,\lambda,z,m)$ is the corresponding climatological mean value for the month m with m=January,…, December. Since the individual sensors cover only partially the same periods, the corresponding seasonal cycles have to be computed for different reference periods as follows: GOME (1996-2002), SCIAMACHY (2005-2010), OMI (2005-2020), GOME-2A (2007-2016), GOME-2B (2015-2020). Before merging the anomlies additive offsets w.r.t. OMI anomalies have to be computed and applied in order to account for biases due to different reference periods. These offsets are obtained from the overlap periods and depend on latitude, longitude, and altitude. One exception is the GOME sensor, which lost its global coverage in June 2003. That means for the overlap period with OMI (2004-2011) additive offsets cannot be derived globally, i.e. for each latitude-longitude grid cell. Instead, mean offsets representative for 5 broadband latitude belts (90°N-60°N, 60°N-30°N, 30°N-30°S, 30°S-60°S, and 60°S-90°S) are computed and added to the GOME anomalies. After the application of the offsets, the merged ozone profile for each spatio-temporal bin is obtained from the median of all available instruments as :

$$\Delta O_{3,mer}(\varphi,\lambda,z,t) = \text{median}(\Delta O_{3,i}(\varphi,\lambda,z,t))$$

Equation 3-4

Corresponding uncertainties of the merged data are estimated using the same approach as used for the merged ozone profiles based on limb satellite sensors (MEGRIDOP) as described in Sofieva et al. (2021). Figure 3-1 shows the anomalies 1995-2022 for all sensors for the latitude/longitude bin 12.5°N/0.5°E and for altitude 20km. In addition, the adjusted anomalies for GOME, GOME-2A, and GOME-2B are shown. Finally, in order to reconstruct absolute ozone values, the seasonal cycle obtained from OMI measurements is used and added back to the anomalies:

$$O_{3,mer}(\varphi,\lambda,z,t) = \Delta O_{3,mer}(\varphi,\lambda,z,t) + O_{3,\text{omi},c}(\varphi,\lambda,z,m).$$

Equation 3-5

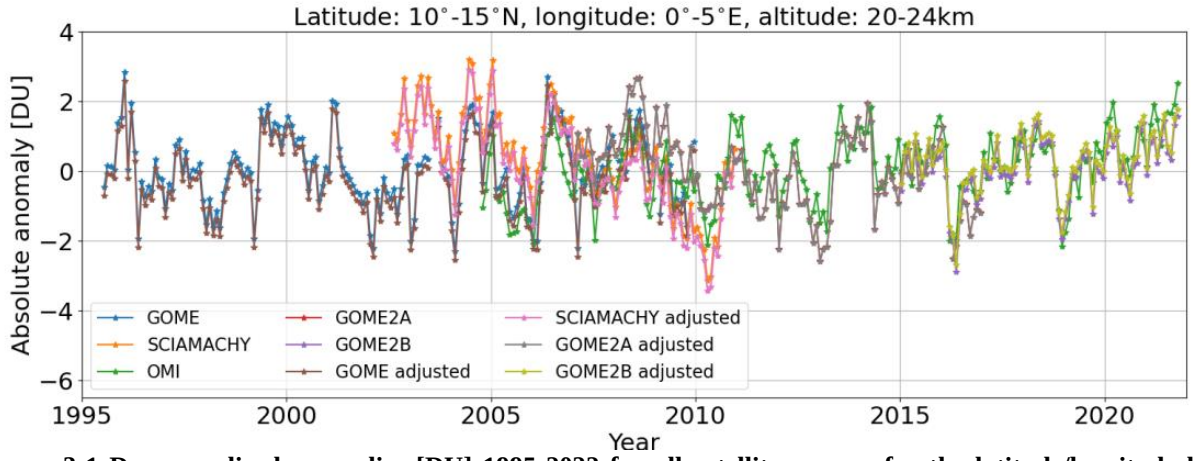

Figure 3-1 Deseasonalized anomalies [DU] 1995-2022 for all satellite sensors for the latitude/longitude bin 12.5°N/0.5°E and for the altitude of 20km. In addition, for GOME, SCIAMACHY, GOME-2A, and GOME-2B the adjusted anomalies w.r.t. OMI anomalies are shown.

3.1.2 Harmonization of merged profiles w.r.t. GTO-ECV total columns

The aim of the harmonization of the merged ozone profiles, generated as described in the previous section, is to achieve consistency between the GTO-ECV total column product and the new GOP-ECV ozone profile record with respect to the total column. The harmonization consists of the following steps:

1. A clustering algorithm is applied to a subset of 80,000 profiles randomly selected from the entire merged data record. We use the same *k*-means clustering procedure as described in Xu et al. (2017) and applied to a set of ozone profiles. From this study we also adopt the optimal number of clusters: K=11. Figure 3-2 shows the output of the clustering: the ozone profiles in each class. Colors denote the total column of each profile. Profiles of similar shapes are grouped into the same class. Class 11 contains mainly profiles from the Northern Hemisphere middle latitudes in boreal spring (maximum total ozone columns >400DU) and class 01 contains mostly profiles from high latitudes in the Southern Hemisphere from September to November (ozone hole season).
2. For each class of ozone profiles a separate Neural Network is trained using as input the total ozone column and as output the corresponding ozone profile shape. The NNs comprise two hidden layers. From the NN training we extract the derivatives for each class, which provide the information about the altitude-dependent change of the profile, when the total column changes. Figure 3-3 exemplarily shows the derivatives for class 03. The shape of the derivatives depends on the total column, and derivatives can be negative.
3. In order to assign one of the 11 classes to each of the remaining profiles, which were not used for the clustering procedure (step (1)), a *k*-nearest neighbors classifier method is applied. The training data set for the classifier contains the profiles of the 11 clusters and the class label (1, …, 11). The fitted classifier is then applied to the remaining profiles in order to predict the corresponding class label, which is needed to select the correct set of derivatives for the altitude-dependent scaling.
4. The last step is the application of the scaling procedure to all merged profiles. The difference ΔTOZ between the total column from the integrated profile and the corresponding total column from the GTO-ECV data record is computed for each spatiotemporal bin and the adjusted profile is computed as follows:

$$O_{3,new}(\varphi,\lambda,z,t) = O_{3,mer}(\varphi,\lambda,z,t) + \Delta TOZ(\varphi,\lambda,t) * d/dTOZ(z),$$

Equation 3-6

$O_{3,mer}(\varphi,\lambda,z,t)$ denotes the merged profile from Sect. 3.1.1, $O_{3,new}(\varphi,\lambda,z,t)$ is the adjusted profile which is consistent with GTO-ECV, and d/dTOZ(z) is the derivative derived from the NN in step (2).

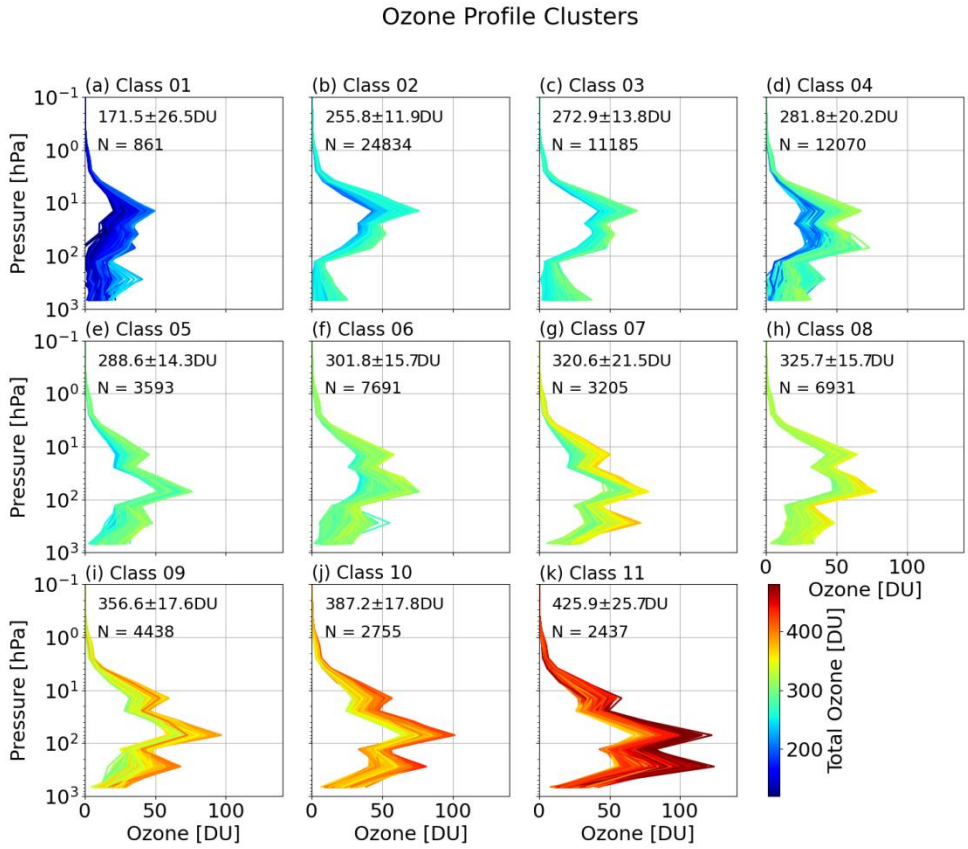

Figure 3-2 Merged ozone profiles grouped in 11 classes using a *k*-means clustering procedure. The total number of profiles is 80,000 randomly selected from the entire data record. Colors denote the total column of each profile.

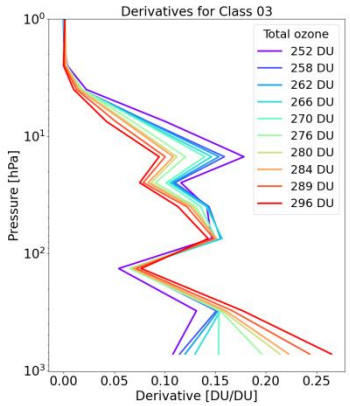

Figure 3-3 Derivatives extracted from the NN training for class 03 (see Figure 3-2). Colors denote the total column.

3.2 RAL nadir profile ECV retrieval algorithms (RAL)

This section is not updated since ATBD V2.1 from CCI+ phase 1. A re-engineered version of the scheme has been developed but results from this scheme are not yet finalised for public release. The re-engineered scheme is described in a separate project internal document (to be made available publically with the release of the updated products).

The RAL profile scheme applied to GOME, GOME-2, SCIAMACHY and OMI within the CCI and C3S is described in ATBDs [RD-54], [RD-53], as well as [RD-33], [RD-42] and [RD-32]. The scheme is also currently being developed for application to Sentinel 4 and 5 via ESA contracts and documented via related ATBDs [RD-45] and [RD-43]. In general, the scheme applies the optimal estimation approach to retrieve the ozone profile in two main steps:

1. "B1 fit": Fit ozone profile to the sun-normalised radiance in the Harley band (in GOME Band 1) from 265-307nm. This provides information mainly on the stratospheric profile and requires good absolute calibration of the sun-normalised radiance spectra. Soft calibration of the B1 L1 radiances in usually required (i.e. radiances are corrected based on differences between L1 radiances and calculated spectra based on radiative transfer calculations from prior knowledge of the ozone distribution).

2. "B2 fit": Add information on tropospheric ozone from the Huggins bands (320-340nm) using the result from step 1) as prior constraint. This requires fitting of differential structure to precision better than 0.1% (close to the noise level) to allow the ozone absorption cross-section temperature dependence to be exploited for tropospheric information (though the requirements on absolute radiometic calibration are less stringent). Extremely good knowledge of the instrument spectral response function is critical for this step.

Work within CCI+ focuses on the application of the algorithm to new sensors GOME-2 Metop C and S5P. For S5P several advances made for Sentinel 4 and 5 will be exploited, in particular:

- The core radiative transfer model is LIDORT [RD-47].

- The speed of the forward model is greatly increased using a "PCFM" approach which requires the core RTM to be run for only a few monochromatic spectral points.

- The B1 uv soft-calibration approach will be based on that developed for S5 [RD-43], based on calculations based on ERA5 meteorology and ozone climatology.

- A new approach to mitigate scene inhomogeneity effects on the spectral response function will be tested using an approach developed for S4 [RD-45].

3.3 IASI FORLI Level-2 Ozone profile retrieval algorithm (ULB)

The IASI ozone profile data product is based on the FORLI (Fast Optimal/Operational Retrieval on Layers for IASI) algorithm. FORLI is a line-by-line radiative transfer model capable of processing in near-real-time the numerous radiance measurements made by the high-spatial and high-spectral resolution IASI, with the objective to provide global concentration distributions of atmospheric trace gases.

The FORLI-O3 v20151001 product was developed and validated during the Ozone_cci Phase-II and constitutes the reference product from 1 October 2007 to 11 December 2019. That IASI/Metop-A FORLI-O_3 dataset has been extensively validated in [RD-11] and [RD-24]. The FORLI software v20151001 [RD-60] was implemented at EUMETSAT in 2019 and the IASI O_3 product is operational at EUMETSAT and distributed via Eumetcast in BUFR format since 4 December 2019. The Eumetsat IASI O3 BUFR files are reformatted in netcdf format by LATMOS and are now distributed by AERIS. They constitute the new CCI database from 4 December 2019. Hence, we recommend to use the ULB-LATMOS FORLI-v20151001 dataset from 20071001 to 20191204 and the EUMETSAT FORLI-v20151001 dataset afterwards, both being available on the Aeris portal at: http://iasi.aeris-data.fr/O3/

An updated FORLI-O_3 v20191122 is now used for the processing of the IASI dataset from 12 December 2019 till present. The backprocessing of the whole IASI dataset at ULB with the last v20191122 is done and will be archived on the Aeris portal in the future.

Finally, a climate data record of IASI O3 (IASI-O3 Level 2 CDR – Metop-A and Metop-B) has been generated at Eumetsat using a climate version of FORLI-O3 (v20151001). It consists of a fully homogeneous record of IASI O3 profiles retrieved from the FORLI-O3 v20151001 using the homogeneous reprocessed IASI-A L1c radiances (from the 10th of July 2007 until the 31st of December 2016; the operational IASI-A L1c data are used onwards) and the operational IASI-B L1c radiances, with the homogeneous temperature and humidity profiles taken from EUMETSAT L2 CDR. For the moment, the IASI-O3 Level 2 CDR from Eumetsat contains only 4 days per month (1st, 8th, 15th, 22nd) over the IASI period. It is reconstructed for ease of use and reformatted by LATMOS.

This part describes the methods used for FORLI (most is extracted from [RD-23]) and is an update of the Ozone_cci ATBD Phase-II. We refer the readers to the Ozone_cci ATBD Phase-II when the section remains unchanged.

3.3.1 Basic retrieval equations

Refer to the Ozone_cci_ATBD_Phase2_V2

3.3.2 Assumptions, grid and sequence of operations

Spectral ranges

FORLI-O_3 (v20151001 and v20191122) uses the Level1C radiances disseminated by EumetCast.

A subset of the spectral range, covering 1025–1075 cm^{-1}, is used for the O_3 retrieval. The spectral range used in the forward model is 960-1075 cm^{-1} and the spectral oversampling is 100.

Vertical grid

FORLI-O_3 uses a vertical altitude grid in km with 1-km tick layers as discretization of the atmosphere

Ozone state vector

The ozone product from FORLI is a profile retrieved on 40 1km-thick layers between surface and 40 km, with an extra layer from 40 to TOA considered at 60 km.

The *a priori* profile $\mathbf{x_a}$ covariance matrix $\mathbf{S}_a$ are constructed from the McPeters/Labow/Logan climatology of ozone profiles (McPeters et al., 2007), which combines long-term satellite limb measurements (from SAGE II and Aura MLS) and measurements from ozone sondes. The *a priori* profile $\mathbf{x}_a$ is the mean of the ensemble. Figure 3-4 illustrates this *a priori* information: the *a priori* profile $\mathbf{x}_a$ has values slowly increasing from around 25 ppbv at the surface to 100 ppbv at 10km, reaching a maximum of 7.3 ppmv in the middle stratosphere. The variability (taken hereafter as the square root of the variance, i.e. of the diagonal elements of $\mathbf{S}_a$) is below 30% in the boundary layer and the free troposphere; it is maximum in the upper troposphere–lower stratosphere, between 10 and 20 km, where it is of the order of 60%. There is significant correlations between the concentrations in the layers 0–10, 10–25 and 25–40 km, but weak correlation between these three (Figure 3-4).

Other state vector elements

Besides the ozone profile, surface temperature and the water vapour column are retrieved.

Measurement covariance matrix

$\mathbf{S}_\eta$ is taken diagonal. The value of the noise is wavenumber dependent in the spectral range used for the retrieval, varying around 2 x 10^{-8} W/(cm^2 .cm^{-1} .sr).

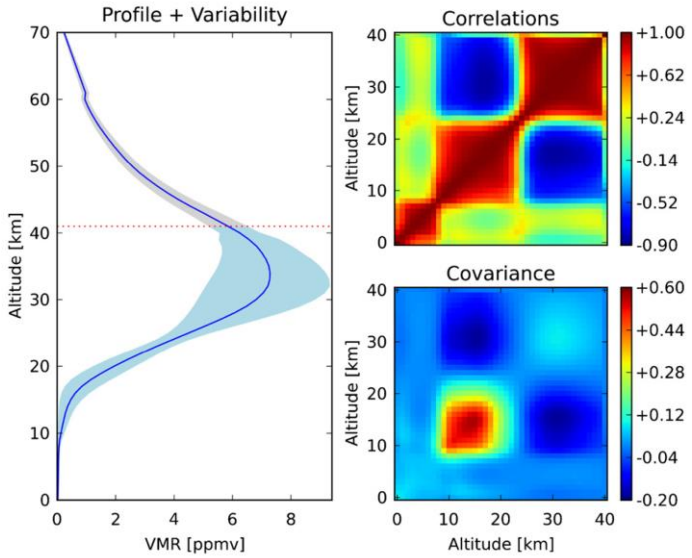

Figure 3-4. Left: x_a (ppmv, blue line) and associated variance (shaded blue) used by FORLI-O3. The dashed red line indicates the top altitude of the last retrieved layer. Right: correlations and S_a variance–covariance matrices in unitless multiplicative factor (from Hurtmans et al. 2012).

3.3.3 Iterations and convergence

Refer to Ozone_cci_ATBD_Phase2_V2

3.3.4 Forward model

Atmospheric state input to the RTM

L1C radiances

FORLI-O_3 uses the Level1C radiances disseminated by EumetCast. A subset of the spectral range, covering 1025–1075 cm^{-1}, is used for the O_3 retrieval.

Temperature and humidity profiles

Profiles of temperature and humidity are from the IASI L2 PPF [RD-61] for both FORLI-v20151001 and FORLI-v20191122, while they are taken from the ERA-5 reanalysis for FORLI-Climate. The atmospheric temperatures are kept fixed whereas the water profile is used as a priori and further adjusted.

Surface temperature

Surface temperatures (land and sea) are from the IASI L2 PPF (FORLI-v20151001 and –v20191122) or from the IASI L2 CDR (IASI-O3 Level 2 CDR). Surface temperature is part of the parameters to be retrieved.

Cloud fraction

FORLI-O_3 (v20151001 and v20191122) uses the cloud fraction from the IASI L2 PPF. All pixels with a cloud fraction equal to or lower than 13 % are processed.

CO_2 profile

FORLI-O_3 v20151001 assumes a constant vertical profile at 380 ppm for CO_2, while the new FORLI-O_3 v20191122 considers time-varying CO_2 concentrations according to the Keeling curve.

Orography

Orography is from the GTOPO30 global digital elevation model and is integrated in the entire IASI FOV (http://eros.usgs.gov/#/Find_Data/Products_and_Data_Available/gtopo30_info).

Emissivity

A wavenumber-dependent surface emissivity above continental surfaces is used while for ocean a single standard emissivity is considered. For continental surfaces, it relies on the climatology of Zhou et al. (2011). In cases of missing values in the Zhou et al. climatology, the MODIS climatology of Wan (2008) is used. It is available on a finer 0.05° × 0.05° grid but is restricted to only 12 channels in the IASI spectral range. In order to deal with this, the spectrally resolved mean emissivity of the Zhou climatology is scaled to match as closely as possible the values in these 12 channels and it is this resulting emissivity that is considered. Finally when there is no correspondence between the IASI FOV and either climatologies, then the mean emissivity of the Zhou climatology is used.

Lookup-tables

Tabulated absorption cross-sections at various pressures and temperatures are used to speed up the radiative transfer calculation. The spectral range for the LUTs used in FORLI-O3 is 960-1075 cm^{-1} and the spectral oversampling is 100. The absorption cross-sections are computed on a logarithmic grid for pressure from 4.5×10^{-5} to 1 atm with a grid step of 0.2 for the logarithm of pressure, and on a linear grid for temperature (162.8–322.6 K with a grid step of 5K). Relative humidity is also introduced in the LUT, varying linearly between 0 and 100%, by steps of 10%.

FORLI-O_3 v20191122 has undergone corrections in the computation of the look-up tables.

Spectroscopy

Line integrated absorption cross section, air broadening, self-broadening, line shifting and absorption cross section data are taken from the widely used HITRAN spectroscopic database version 2008 (Rothman et al., 2009). Continuum formulations are taken from MT-CKD (Clough et al., 2005).

The last FORLI versions (v20191122 and FORLI-Climate) uses the Hitran database update to the latest available version with largely corrected CO line intensities and positions and also updates for HNO_3, as well as MT_CKD update and the related use of Line-Mixing for CO_2 lines.

Note that other corrections have also been implemented: altitudes computation, correct usage of humidity …

Radiative Transfer Model (RTM)

Refer to Ozone_cci_ATBD_Phase2 for a full description of the RTM (general formulations and numerical approximations).

3.3.5 Error description

Refer to Ozone_cci_ATBD_Phase2.

3.3.6 Output product description

Formats

The FORLI-O_3 retrieval datasets for IASI-A, -B and -C processed with the ULB-LATMOS FORLI-O_3 v20151001 from 1 October 2007 to 4 December 2019 and with the EUMETSAT FORLI-O3 v20151001 dataset afterwards till present are delivered in NetCDF (v4) format and can be downloaded from the Aeris portal at: http://iasi.aeris-data.fr/O3.

Ozone profile and characterization

The ozone product from FORLI is a profile retrieved on 40 layers between surface and 40 km, with an extra layer from 40 km to the top of the atmosphere (TOA) considered at 60 km. The dataset includes O_3 total columns along with vertical profiles. It also includes other relevant information such as the a priori profile, the total error profile and the averaging kernel (AK) matrix, on the same vertical grid.

3.3.7 Retrievals and Quality flags

A series of Quality input and processing flags were applied to the FORLI-O_3 (v20151001 and v20191122) datasets to exclude bad quality data, specifically when:

(i) The input values (T, Q, Cloud) are missing, or in case of negative surface altitudes or unrealistic skin temperature

(ii) The spectral fit residual root mean square error (RMS) is higher than 3.5×10^{-8} W/(cm^2 sr cm^{-1}), reflecting a too large difference between observed and simulated radiances

(iii) The spectral fit residual bias is lower than -0.75×10^{-9} W/(cm^2 sr cm^{-1}) or higher than 1.25×10^{-9} W/(cm^2 sr cm^{-1})

(iv) The spectral fit residual is sloped

(v) The partial O_3 column or the humidity is negative

(vi) There were abnormal averaging kernel values. These are identified checking for unrealistic values – larger than 2 – or unrealistic strong gradient/oscillation on the averaging kernel profiles)

(vii) The spectral fit diverged or reached a fixed maximum number of iterations without converging, or the Chi-Square value is too high
(viii) The total error covariance matrix is ill conditioned.
(ix) No retrieval is done due to incorrect inputs or other reasons

For an optimal use of the data (e.g. for validation application), users should also exclude data when:

(i) The O_3 profiles have an unrealistic C-shape (i.e. abnormal increase in O_3 at the surface, e.g. over desert due to emissivity issue), with a ratio of the surface – 6 km column to the total column higher or equal to 0.085
(ii) The DOFS is lower than 2, which are mostly associated with bad quality data in the Antarctic region.

3.4 Merged IASI-A, -B and -C Level 3 ozone profile dataset (FORLI v20191122)

The results from previous phases of the CCI project showed an excellent consistency between the IASI-A, -B and -C ozone profile retrievals by the standard FORLI-O3 algorithm (v20191122). In this phase, we develop a scheme to merge the three IASI ozone profile data records (with associated error and total ozone column averaging kernel). The merged IASI O3 profile in a level-3 grid cell is a weighted average of all IASI-A (from 20080101 to 20190919), -B (from 20130308 to now) and -C (from 20190920 to now) O3 profiles assigned to that grid cell and for each retrieved layers. The total retrieval random error (i.e. measurement and smoothing errors) are considered for the weighted averaging and for the corresponding standard error in the bin:

$$Weighted\_Mean = \frac{\sum_i \frac{x_i}{\sigma_i^2}}{\sum_i \frac{1}{\sigma_i^2}}$$

$$Standard\_Error = \sqrt{\frac{1}{\sum_i \frac{1}{\sigma_i^2}}}$$

Where σ_i are the random uncertainties reported by the FORLI-O3 (20191122) retrieval algorithm corresponding to all individual retrieved ozone values from IASI-A, -B and -C in the bin.

3.5 Combined uv/vis/thermal-ir retrieval algorithm (RAL)

This section is not updated since ATBD V2.1 from CCI+ phase 1.

3.5.1 Overview

Within CCI+ (mainly in year 2) RAL will investigate improve the information content of the GOME-2 nadir ozone profiles by adding information from (i) the visibile Chappuis band (also measured by GOME-2) and (ii) thermal IR measurements by IASI (ii). The approach is to combine information from indendent level 2 (L2) retrievals from the different spectral ranges, i.e. adopting a so-called "L2-L2" combination approach. Sections below described the Chappuis and IR retrieval schemes to be employed, following by an overview of the L2 combination methodology.

3.5.2 Chappuis retrieval scheme

The potential advantages of using the Chappuis bands (440-700nm) are well known [RD-13]: The Chappuis absorption is generally optically thin with very little temperature dependence. There is consequently little sensitivity to vertical profile shape (only total column information can be retrieved from the Chappuis band alone). However it can complement the uv measurements of total ozone because near-ground sensitivity to ozone in the Huggins bands is limited by the typically low surface reflectance and Rayleigh / aerosol scattering. In the Chappuis range, the albedo over land is typically larger and Rayleigh scattering much reduced, so that a larger proportion of the observed photons will have passed through the lowest atmospheric layers. Extracting the signal from the Chappuis bands is complicated by the fact that the amplitude of differential structures (which are exploited by DOAS techniques) are relatively low and have a relatively broad band structure compared to the features in the Huggins bands. Such features may be easily confused with a number of other effects e.g. instrumental artefacts (such as polarisation sensitivity, aliasing of spatial/spectral structure due to non-synchronous detector pixel read-out) and spectral variations in surface reflectance. In addition, there are contaminating spectral features from water vapour (H2O), oxygen dimer (O4) and nitrogen dioxide (NO2). Although Rayleigh scattering is reduced, the Ring effect (due to inelastic scattering by air molecules) is still significant. Inelastic scattering at the ocean surface is also important over sea, although in conditions where this is important, the information content of the Chappuis bands is less useful (as the ocean surface reflection is very low).

Via UK National Centre for Earth Observation (NCEO) funded work (to be consolidated in the coming months) two approaches have been developed to extract the total (slant) column of ozone from the Chappuis: (1) A DOAS based approach, which has a directly physical basis. This involves fitting absorption cross sections for all relevant gases and scale factors for terms related to known surface spectral variability and other known effects (Ring effect, spectral shifts, instrument polarisation features etc); (2) A statistical approach based on regressing the Chappuis band measurements to the ozone slant column retrieved from the Huggins bands. This involves determine singular vectors of the Chappuis band spectral variability which is uncorrelated with the total ozone variability enabling total ozone to be retrieved along with spatial patterns which are related to other physical variables. In both cases the slant column of ozone is estimated. The sensitivity of the slant column to height resolved perturbations in ozone can be calculated, forming effectively the averaging kernel of the retrieved slant column with respect to changes in ozone

profile. This information can then be combined with the uv retrieval using the L2-L2 approach outlined below.

Further details of the consolidated approach will be given in the next version of this ATBD.

3.5.3 RAL Infra-red / Microwave sounder retrievals

Also within NCEO and supported by Eumetsat studies, RAL have developed an infra-red microwave sounder (IMS) scheme which retrieves ozone profiles along with temperature, humidity and other atmospheric variables from Metop IASI, AMSU and MHS. Products from the scheme have been validated in CCI+ Water Vapour and will be used to generate a combined limb/nadir sounder product in that project. The scheme is described in the CCI+ water vapour ATBD [RD-44], though the current version of the scheme uses an extended set of channels to improve the sensitivity to the ozone profile. The scheme is based on optimal estimation and provides all the necessary information to enable L2-L2 combination with the uv profiles as described below.

3.5.4 L2 L2 Combination

LThe L2-L2 combination is implemented by posing the problem as a linear retrieval in which we wish to optimally estimate a profile by combining the information contained in different retrievals. The approach should work for a retrieval of any property linearly related to the profile e.g. (sub-)column amounts or mixing ratio profiles on a coarsely sampled vertical grid (provided the transformation to a fine grid is clearly defined). For the approach to work, it is assumed that averaging kernels are provided (or can be constructed) for all input retrievals, with respect to fine scale perturbations in the true profile (defined in the same units on the same finely resolved grid).

We choose to represent the (output, optimised) profile in a flexible way on a fine vertical grid using N basis functions (this can be different from the way the input retrievals represent the profile):

$$r(z) = o(z) + \sum_{i=1,N} x_i B_i(z)$$

Equation 3-7

Where $o(z)$ is an “offset” profile (which can be considered as the new prior profile on the fine grid). $B(z)$ are a set of suitable basis functions (e.g. triangular functions representing linear interpolation from a coarse vertical grid, or principal components of the assumed profile variability etc). The N element vector $x$contains state vector elements to be retrieved.

Alternatively, considering vector r to describe the profile on a finely resolved vertical grid:

$$r = o + Bx$$

Equation 3-8

Where B is a matrix containing the N basis functions.

The optimal x (and hence r) can be obtained using the input retrievals as the "measurements" for an OEM retrieval. These are contained in a measurement vector, y. We can relate each to r, using the averaging kernels as the forward model function:

$$y_j = A_j(r - r_{aj}) + a_j$$

Equation 3-9

Where index j represents a specific sub-column amount (from TIR or SWIR). A_j is the averaging kernel (vector) for this sub-column (from the TIR or SWIR retrieval), describing the derivative of the sub-column with respect to perturbations *on the fine grid*. r_{aj} is the (finely resolved) prior profile used in the previous (input) retrieval and a_j is the corresponding prior sub-column amount.

Substituting for r gives

$$y_j = A_j(o + Bx - r_{aj}) + a_j$$

Equation 3-10

Using this (linear) forward model for $F(x), x$ can be estimated via minimisation of the usual cost function, χ^2, i.e.

$$\chi^2 = (x - x_a)^T S_a^{-1}(x - x_a) + \big(y - F(x)\big)^T S_e^{-1}\big(y - F(x)\big),$$

Equation 3-11

Where the measurement covariance S_e constains the estimated error covariances of the (TIR+SWIR) subcolumns in y**.** *A priori* covariance S_a describes the estimated prior errors on the state vector (i.e. the basis function weights). In principle these are defined to represent realistic prior knowledge in the profile, though tuning to match the information content of the joint retrieval is likely to be needed in practise. The prior state itself, x_a , is typically a vector of 0s, since the state describes increments to the offset profile, o.

Since the forward model is linear, the solution which minimises the cost function is given by

$$\hat{x} = x_a + (K^T S_e^{-1} K + S_a^{-1})^{-1} K^T S_e^{-1}\big(y - F(x_a)\big)$$

Equation 3-12

where weighting function matrix K is the derivative of the forward model with respect to the state parameters, i.e.

$$K = AB$$

Equation 3-13

Where **A** is the matrix containing the averaging kernels of the input retrieved amounts with respect to the fine scale profile (columns are A_j in Equation 3-10). Note that (assuming linearity), using the averaging kernel equation as the forward model operator, effectively removes the influence of the original retrievals prior constraint on the joint retrieval (this is effectively replaced by the new prior).

Given the solution state, it is trivial to compute the corresponding high-resolution version of the profile, r (Equation 3-8). Sub-column amounts for specific layers can then be calculated from that

profile. This step can be carried out by matrix multiplication by matrix, M, which contains the weights needed to integrated the profile to a set of sub-column amounts, such that

$$s = Mr$$

Equation 3-14

Via the usual OEM equations, the total a posteriori errors on $\hat{x}$ are described by covariance

$$S_x = (K^T S_e^{-1} K + S_a^{-1})^{-1}$$

Equation 3-15

The (non-square) averaging kernel for $\hat{x}$, giving derivatives of the solution with respect to *fine-scale* perturbations in the profile is given by

$$A_x = S_x K^T S_e^{-1} A$$

Equation 3-16

(A, without subscript, is the derivative of the input retrievals with respect to fine-scale perturbations in the true profile).

The (square) averaging kernel for the output fine scale profile is:

$$A_r = B A_x$$

Equation 3-17

The (non-square) averaging kernel for the derived sub-columns (with respect to fine scale perturbations in the profile) is

$$A_s = M A_r$$

Equation 3-18

Errors on the retrieval profile and sub-columns are described by covariances:

$$S_r = B S_x B^T$$

Equation 3-19

$$S_s = (MB) S_x$$

Equation 3-20

(The noise and smoothing error covariances can be similarly derived starting from the usual OEM expression for these matrices for the state vector $\hat{x}$**).**

4 Limb profile ECV Retrieval / Merging Algorithm

4.1 OMPS-LP IUP retrieval algorithm

We provide here an overview of the preliminary version of the UBR-IUP retrieval for observations from OMPS-LP on board NOAA-21 (N21). This retrieval version shares the same approach based on spectral fitting and similar settings with the ozone retrieval implemented for OMPS-LP onboard Suomi NPP. It implements a first-order Tikhonov regularization within the SCIATRAN radiative transfer model. As described in [RD-59], five spectral segments are selected: three in the Hartley and Huggins bands and two in the visible spectral range. We have to take into account the presence of water vapor and O_2 absorption features in the Chappuis band used for the lowest altitude range (*) so that wavelengths in the intervals 585-605 nm and 620-635 nm are rejected. The treatment of these absorption features requires line-by-line calculations, which are computationally expensive to be implemented for the whole time series.

Considering the decreasing sensitivity above 55 km and the saturation of limb signal in the lower stratosphere, the retrieval of ozone profiles is performed over the altitude range between 8.5 and 60.5 km, with the lower boundary that can be higher in the presence of a cloud. An evenly spaced vertical grid spans this vertical range with steps every 1 km.

The measurement vector consists of the logarithms of the normalized limb reflectance (sun-normalized radiance). In detail, OMPS-LP spectrum in the five spectral segments at each altitude is normalized by a limb measurement at an upper TH. This provides a self-calibration of the instrument and reduces the effects of surface/cloud reflectance uncertainties. Table 4-1 lists the details about spectral segments and the used normalization altitudes.

For each TH a polynomial is subtracted from the logarithm of the normalized radiance to remove slowly variable spectral features, for example, related to Rayleigh or aerosol scattering. The last column of Table 4-1 provides information about the order of the polynomial subtracted: zeroth order or no polynomial in the UV region and first order for the Chappuis band.

TH [km]	Spectral segment [nm]	Normalization TH [km]	Poly. order
48-60	290-302	62.5	-
34-49	305-313	51.5	-
28-39	321-330	51.5	0
16-31	508-660	42.5	1
8-16 (*)	508-670	42.5	1

Table 4-1: ***List of the spectral segments considered for the ozone retrieval with corresponding TH ranges, altitudes used for the normalization and order of the subtracted polynomial.***

As O_3, NO_2 and O_4 have relevant spectral signatures in the selected spectral ranges, the radiation field in the forward model is calculated, taking into account these three gases. The respective cross-sections are taken from [RD-41], [RD-10] and [RD-21] and are beforehand convolved to the OMPS-LP spectral resolution.

Surface albedo is retrieved simultaneously, by assuming a Lambertian surface and using the sun-normalized radiance. For the aerosol retrieval, it was not possible to develop an ad-hoc extinction product for N21, so that the aerosol information used in the ozone retrieval is taken from the extinction profiles retrieved from Suomi NPP observations. Aerosol profiles are daily and zonally averaged and used in the N21 ozone retrieval. This approximation is estimated to impact only the lowermost stratosphere, with an average discrepancy of about 2-5 % below 17 km.

The NASA team so far provided a preliminary version of L1G data, which include static pointing adjustments tuned to the N21 instrument, and also intra-orbital dynamic pointing corrections that are the same implemented for the Suomi NPP instrument. Only the central slit of the instrument has been processed so far.

4.2 High-resolution gap-free dataset of ozone profiles

The high-resolution gap-free dataset of ozone profiles is daily gridded profiles in the pressure range from 900 to 0.02 hPa with the horizontal resolution of 1°x 1°. It covers year from 2002 to present. The dataset is created using the ozone profiles data from MLS, OSIRIS, GOMOS, MIPAS, SCIAMACHY, OMPS-LP, ACE-FTS, and SAGE III/ISS.

The details of data processing are provided in [RD-65]. In our algorithm, the creation of homogenized interpolated dataset of ozone profiles consists of three main steps:

(1) Homogenization of ozone profile data from the limb satellites measurements;
(2) Interpolation of the limb profiles from each day to 1°x1° horizontal grid;
(3) A smooth transition to the adjusted model data below the tropopause.

In the first step, the data from different satellite instruments are homogenized. We use MLS as a reference dataset. For all other instruments, the biases with respect to MLS are evaluated for each month and for each latitude (with 1° increment), using 10° overlapping zones and corrected via adding latitude-dependent offset. This procedure removes the biases between the limb datasets. After that, we applied a simple approach for validation / a-posteriori estimation of random uncertainties. For each instrument and each month, we evaluated sample variance s^2 in 10° latitude zones from experimental data and the SILAM-adjusted field, which is sub-sampled at measurements locations. This sample variance s^2 provides the estimates of natural variability σ_{nat}^2. Then a posteriori (ex-post in von Clarmann et al. (2020) terminology) uncertainties can be estimated as $\sigma_{ex-post}^2 = s^2 - \sigma_{nat}^2$. We computed latitude and altitude dependent offset $\Delta = \sigma_{ex-post} - \sigma_{ex-ante}$ ($\sigma_{ex-ante}$ is the mean error estimate provided with profiles, in the same 10° latitude zones over the month) and applied it to each profile. By construction, the resulting uncertainty estimates are also compatible with the observed ozone variability.

After homogenization, the limb data are interpolated to form a high-spatial resolution dataset. We apply a kriging-type interpolation, in which both data uncertainty and the structure of the data variability are taken into account. In this approach, the value at the point **r** is taken as a weighted mean of data in the neighbourhood:

$$x(\boldsymbol{r}) = \sum_i w_i \, x(\boldsymbol{r}_i), \quad (1)$$

with the weights w_i inversely proportional to the total uncertainties:

$$\sigma_{tot,i}^2 = \sigma_{noise,i}^2 + D(\boldsymbol{r}_i - \boldsymbol{r}), \quad (2)$$

where σ_{noise}^2 is the estimate of the noise in the data, and $D(\boldsymbol{r}_i - \boldsymbol{r})$ is the uncertainty due to the spatial mismatch, which is usually estimated via the structure function. In our interpolation method, $D(\boldsymbol{r}_i - \boldsymbol{r})$ is taken from the adjusted SILAM field, for each day. The weighted mean is assessed using the 10°x20° latitude -longitude area around each point [RD-65].

The interpolation of ozone profiles is performed at each pressure level separately. An example of the interpolated field is shown in Figure 4-5.

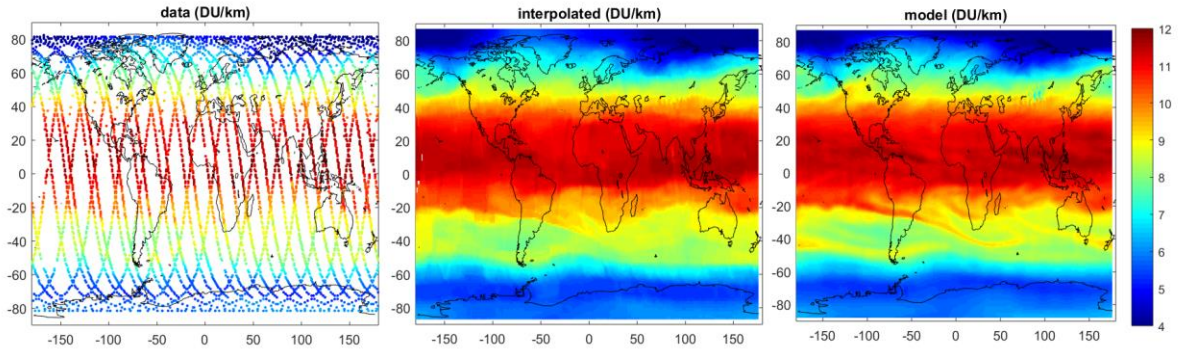

Figure 4-5. Left: ozone at limb satellite measurements at 10 hPa on 1 September 2018. Center: after interpolation. Right: corresponding adjusted SILAM ozone field at the same pressure level.

Since satellite data have limited accuracy, non-homogeneous and rather sparse coverage below the tropopause, we extended the satellite-based ozone profiles to lower altitudes by using the smooth transition to the adjusted SILAM profiles. The linear transition is performed in such a way that above 200 hPa the profile follows fully the experimental data and below 400 hPa - fully the model data. The illustration of the transition to the model data at lower altitudes is shown in Figure 4-6, for tropical and polar atmospheres.

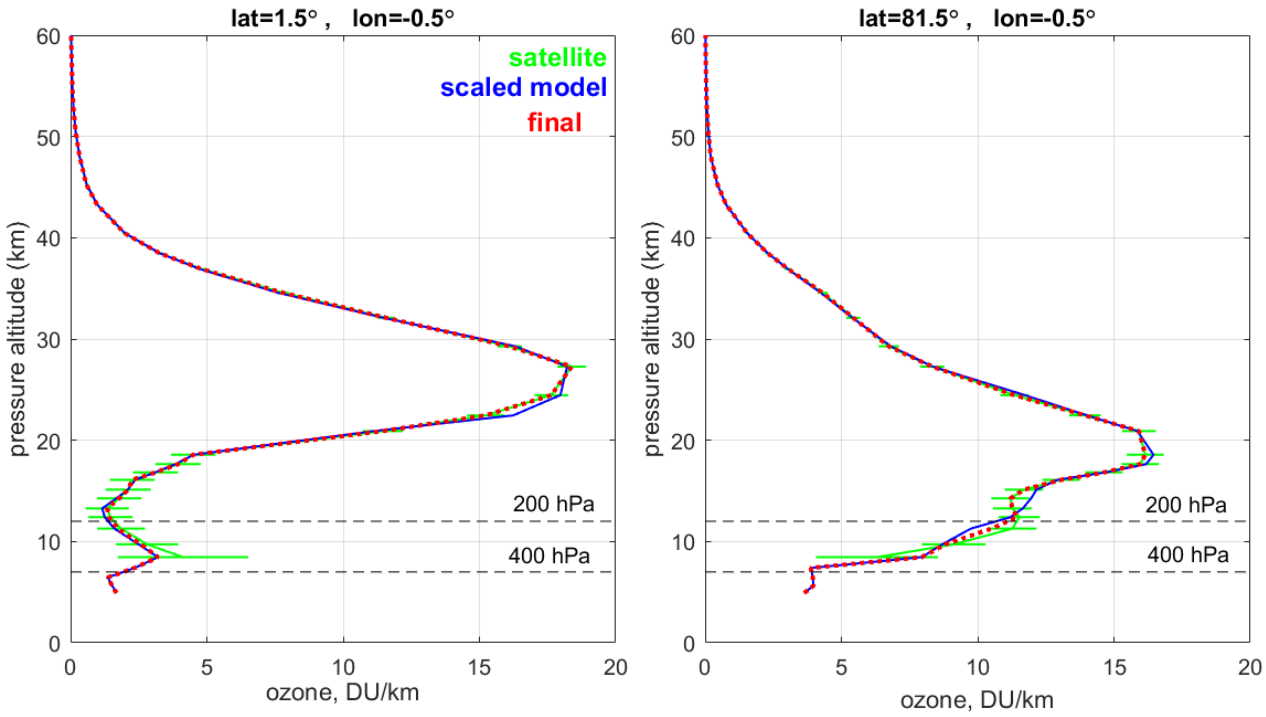

Figure 4-6. Illustration of transition to model-adjusted profiles at lower altitudes for tropical (left) and polar region (right). The vertical coordinate is pressure altitude $z = 16\,log_{10}(P_0/P)$, where P_0=1013 hPa is the standard pressure and P is pressure in hPa.

The resulted ozone profiles are included into the high-resolution gap-free dataset of ozone profiles.

5 Tropospheric Ozone

5.1 Merging of tropical GOME-type CCD data (GTTO-ECV scheme) (DLR)

The convective cloud differential (CCD) algorithm for the tropical tropospheric ozone column (TROC) is based on the level 2 nadir total column ozone products. Tropospheric ozone (TROC) is calculated as the difference between the total ozone column (TOC) for cloud free pixels and the stratospheric column, where the stratospheric column (SOC) is determined as the column above deep convective clouds. Only observation with high cloud cover (c_f > 80%) are taken into account, and to avoid measurements over thin cirrus clouds the cloud albedo has to be higher than 80%. The SOC is given as the difference between the total column and the ozone column below the cloud (ghost column), which is hidden below the clouds and invisible to the instrument.

For Sentinel 5 P the CCD algorithm is part of the operational processing. S5P data are spatially and monthly averaged to have the same resolution as the other sensors. For most other sensors (GOME, SCIAMACHY, OMI, GOME-2A and GOME-2B) an existing algorithm [RD-63] from the former ESA CCI project has been updated and the data were reprocessed, including GOME-2C which had not been part of the former CCI project.

5.1.1 Cloudy observations: SOC

Because the top height of the clouds may differ, even if only clouds with a top height between 8 and 15 km are considered, the above cloud ozone columns are harmonized to a certain pressure level (270 hPa or 200 hPa). The small correction term is calculated by integrating an ozone climatology profile between the effective cloud top and fixed pressure level. The algorithm's idea is illustrated in Figure 5.1. The data are monthly averaged and gridded (1° x 1°). The assumption that the SOC is constant for 1 month limits the algorithm to the tropical ozone data. Moreover, for certain regions or periods no stratospheric data are available or they are affected by up draught of tropospheric ozone pollutions e.g. over the rainforest during the burning season. Therefor only the stratospheric ozone data in a reference region are used, and assumed to be representative for the entire tropics. We indirectly presume that the stratospheric column is constant for certain latitude bands, which is a good approximation for the tropics (20°S to 20°N).

According to Lidar observations (Browell et al., 2001) the upper tropospheric ozone mixing ratio in convective systems over the western Pacific are less than 10 ppb, hence the up draught in this region is low. Moreover, the convective cloud cover is often high. This makes the region over the eastern Indian ocean (70°E) to the western Pacific (170 W) a good reference area. More details are described in [RD-64] or [RD-63]. The cloud slicing algorithm confirms that the up draught ozone mixing ratio inside and above the cloud in the reference area is low, as explained in the first paper.

Due to high number of observations from S5P the period for the SOC could be reduced to 6 days. A 2.5 degree smoothing kernel is applied to the SOC. S5P cloud data are retrieved with OCRA/ROCINN algorithm, that results in slightly lower cloud altitude, hence we set the pressure level to 270 hPa - while we used 200 hPa before. To avoid any inconsistency with either the

operational S5P data or the previous CCI versions we now offer two versions of the dataset. One reaches up to 270hPa and includes the operational S5P. For the second one the top pressure level is set to 200 hPa, We applied the same algorithm to the reprocessed S5P OFFL total ozone columns but the pressure level to 200 hPa.

Compared to the operational S5P tropospheric ozone column, also the input orbits for the individual days differ for the internal reprocessing , leading some noise in the difference, and a bias caused by the different top pressure levels Also the tropospheric ozone columns for all other sensors were reprocessed with both pressure levels.

5.1.2 Cloud free observations: TROC

Total column observations are affected by clouds in a way that the ozone below the cloud is shielded. Therefor cloudy observations approximate the stratospheric column (see above) very well. On the other hand the tropospheric column is only part of the observed total column if the cloud fraction (<0.1) and cloud altitude are low.

For those case the stratospheric column is subtracted from the total column and the tropospheric residual remains. The tropospheric columns are averaged over for 1°x1° and one month. Due to the large pixel size of GOME (320km) the data are "smeared out" over several grid cells and weighted with the longitudinal range within the grid cell. Also the resolution of the GOME-2 instruments (80km) is in the order of 1°, because of that the weighted mean was used here as well.

S5P has a very high resolution and a large coverage, so in the operational dataset the time resolution is reduced to 3 days and spatial resolution to 0.5°x1°.

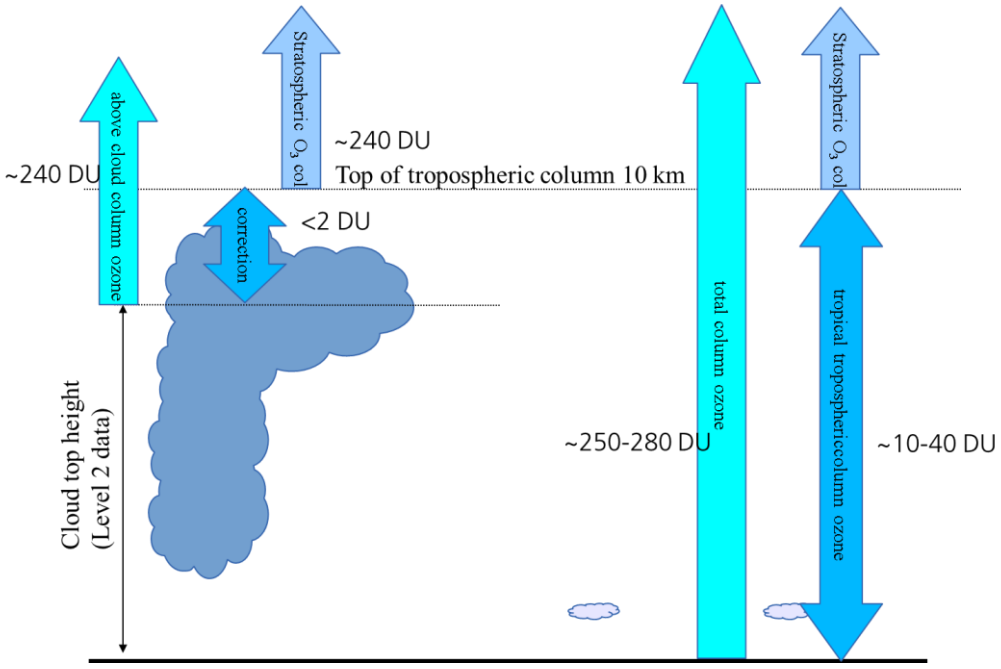

Figure 5.1: Schematic illustration of the CCD technique for the (sub)-tropics. Cloudy satellite observations with cloud fraction cf > 0.8, cloud top albedo ac > 0.8 and cloud top pressure pc > 320hPa, which are used to determine the above-cloud ozone column, are shown on the left. Cloud-free measurements (cf < 0.1) are shown on the right. The resulting difference is a tropical tropospheric ozone column below 270 hPa.

An example of the GOME-2 tropical tropospheric ozone column distribution is shown in Figure 5.2 for September 2008. This figure illustrates the effect of biomass burning on the tropical tropospheric ozone, formaldehyde and NO_2 distribution (GDP-4.8). The bottom right figure shows the southern hemisphere biomass burning hot spots as measured by ATSR in September 2008. The biomass burning produced large amounts of NO_2 over Southern Africa and South America as can be seen in this figure (top left). The largest increases in ozone are found over the southern Atlantic as shown in Figure 5.2 (bottom left), and are a result of the biomass burning emissions and large-scale transport.

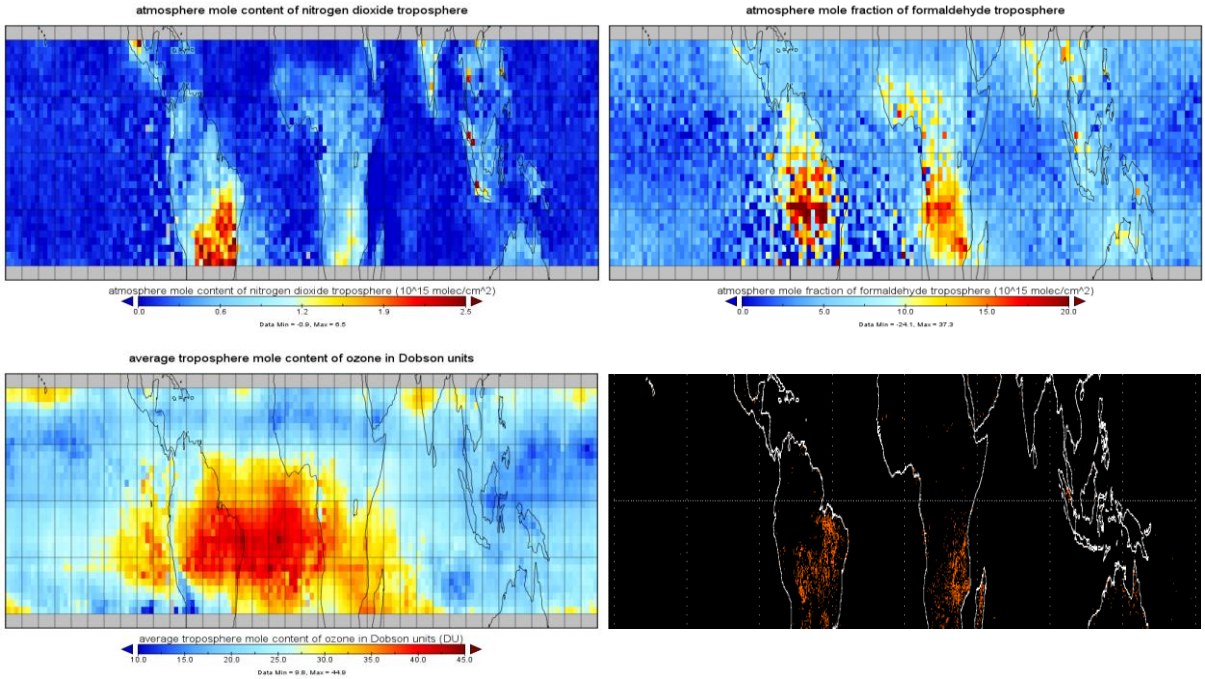

Figure 5.2: Southern hemisphere biomass burning hot spots measured by ATSR (bottom right), and tropospheric NO2 columns (top left), HCHO column (top right) and tropospheric ozone columns (bottom left) as measured by GOME-2A in September, 2008.

5.1.3 Sentinel 5P monthly means

Sentinel 5P tropospheric columns are retrieved operationally as part of the offline processing chain. Here different spatial and temporal resolutions are achieved. For the long term time series such high resolution data set is not practical the data are averaged in both temporal and spatial dimensions.

The daily columns for TROC, SOC and TOC were averaged independent from each other weighted by the number of daily observations. The fact that the daily data files already contain averages over three days is assumed to cancel out for the monthly mean, however, the first and last day of a month might be weighted less in the monthly mean. The number of measurements for each monthly mean pixel is given by the sum of all measurements divided by three - assuming that each daily file contains data from three consecutive days.

The errors of each daily column data propagate into the monthly mean uncertainty by the average of the squares:

$$\sigma_{mean} = \sqrt{\sum_{month} \frac{\sigma_{daily}^2}{month}}$$

In contrast to the CCD data files from the other sensors, the operational S5P data do not contain any cloud information. That is why cloud information is not included in the monthly means and also not provided in the merged data files. The surface altitude and albedo are simply averaged over one month, it is expected that both do not change significantly within this period, for these two quantities no deviations are provided.

5.1.4 Error estimates

Both tropospheric and stratospheric columns represent averages over many individual measurements, having their own uncertainties. However, when averaging over a longer period the spread between the observations dominates over the uncertainty of the individual observation. As long as there are enough cloud free observations (~>10 per grid cell) the error propagated into the final tropospheric column is by a factor of 5 lower than the standard deviation.

The error of the stratospheric column is assumed to be the same as the error of the individual observation for the total column. In the first step the error propagated into the SOC for the cloudy observations over the reference region. In the second step we calculated the final error for the TROC based on the error of the SOC as well as the errors of each TOC observations for cloud free observations. Potential errors in the cloud height or cloud fraction were not included. For some arbitrary selected files, the propagated error varied between 0.3 and 0.6 mmol/m² (~0.6-1.2 DU) the standard deviation for the same files showed a stronger variability and reached up to 6 mmol/m² but were mostly around 3 mmol/m². For the final tropospheric ozone columns both the standard deviation and the error are given as `deviation` and `error` respectively.

5.1.5 Harmonisation of the individual products

All TROC products differ due to the different instruments with some biases or drifts relative to each other, they also cover different periods. We apply the algorithm described below for the time series of monthly tropical mean data.

The longest time series originates from the OMI observations and OMI is known to be very stable with respect to instruments drifts. This qualifies OMI as reference, and all other instruments are harmonised relative to OMI. For the harmonisation the mean bias between the reference and the other instrument is subtracted as well as a mean difference in the annual cycle (Figure 5.3). One can easily show that this is the same as the deseasonalised merging scheme presented in similar tasks above.

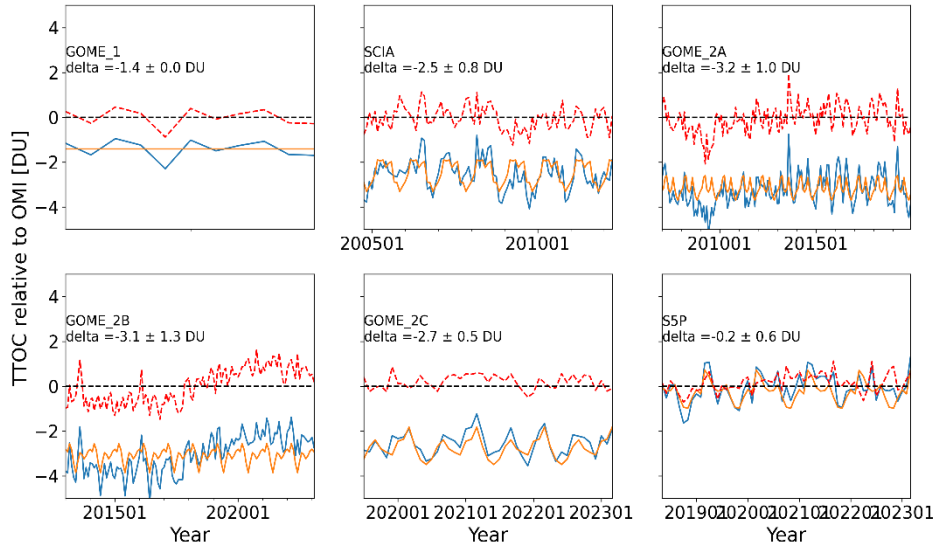

Figure 5.3: Harmonisation of the tropospheric ozone products up to 200 hPa. The blue line shows the difference between the reference (OMI) and the individual sensor. In orange the mean annual cycle difference is shown and the difference of the corrected dataset and the reference is in red. The mean bias is given in the individual figures.

After the tape record failure of ERS-2 in 2003 the GOME data did no longer cover the tropical band. As a consequence, the GOME tropical tropospheric ozone data end in June 2003 and the time series does not overlap with the reference OMI. Moreover, the overlap to SCIAMACHY consists of a 1 year period only. We therefore first harmonised SCIAMACHY relative to OMI and subtracted the mean bias between SCIAMACHY and GOME to harmonise the GOME data. The harmonise data sets are shown in Figure 5.4, at least for the small overlapping period SCIAMACHY and GOME agree quite good, even though the annual cycle was not considered during the harmonisation of GOME relative the harmonised SCIAMACHY data.

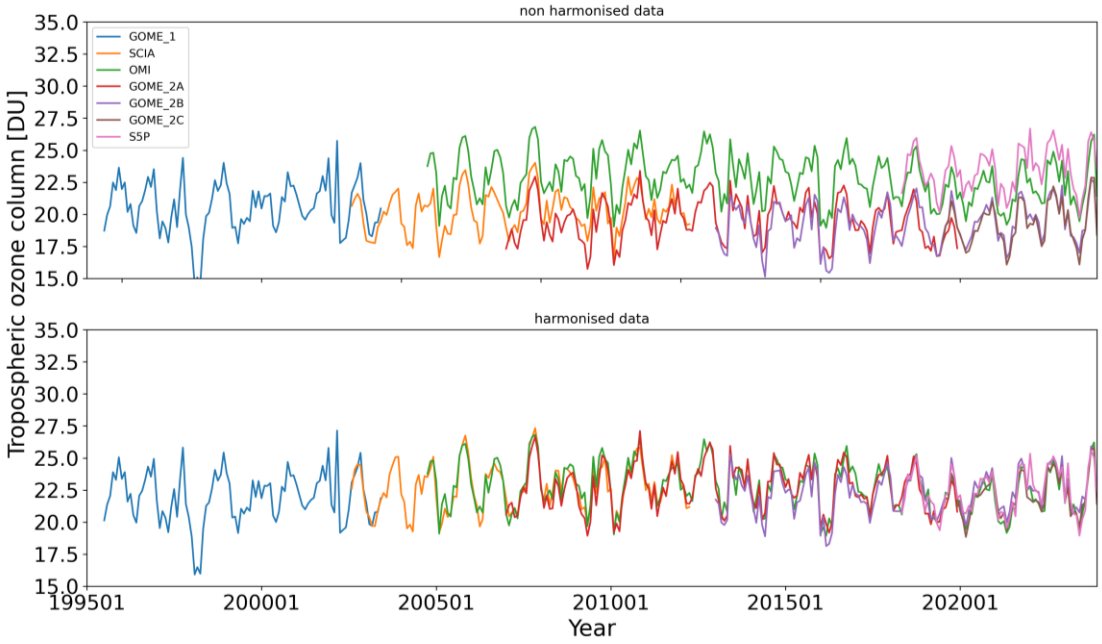

Figure 5.4: time series of tropical mean tropospheric ozone columns before the harmonisation (top) and after the harmonisation (below).

5.1.6 Other variables in the harmonised products

Besides the tropospheric ozone column also the average tropospheric ozone mixing ratio between the surface and the top of the tropospheric column, the stratospheric columns and the total columns are provided in the files.

The tropospheric ozone mixing ratio is scaled according to the harmonisation of the tropospheric column

$$MR_{trop}^{cor} = \frac{MR_{trop} * TROC_{Trop}^{cor}}{TROC_{trop}}$$

While the normalisation of the average mixing ratio is straight forward, the harmonisation of the total and stratospheric column causes an issue. For the CCD the tropospheric column is given as $TROC = TOC - SOC$. After the TROC is harmonised the equation is obviously no longer valid. To avoid the inconsistency at this point we harmonise the stratospheric reference columns in addition to the tropospheric column and defined a new total column as $TOC = TROC + SOC$. The total column in the harmonized tropospheric ozone datasets therefore deviates from the total column dataset in the original (non-harmonised) dataset, and also from most harmonised total column data products.

Error data or surface properties were not harmonised, but simply averaged or propagated respectively.

5.2 Global tropospheric ozone from nadir and multiple limb sensors (FMI)

The tropospheric ozone column from combination of nadir and limb instruments is obtained via the residual method, i.e., from the stratospheric ozone column is subtracted from the total ozone column.

OMI or GTO-ECV are used for total ozone column data. The stratospheric ozone column is computed either from the tropopause or from 3 km below the tropopause using the high-resolution gap-free dataset of ozone profiles (Sect. 4.2).

Once the high-resolution stratospheric ozone column dataset is created, the application of the residual method is straightforward: the stratospheric columns are subtracted from the clear-sky measurements by the nadir sensors, daily. The daily values can be averaged to monthly mean values subsequently.

The illustrations of tropospheric ozone column and associated uncertainties can be found in [RD-65].